Hindawi
Advances in Meteorology
Volume 2023, Article ID 5478666, 18 pages
https://doi.org/10.1155/2023/5478666

Research Article

Estimation of the Total Amount of Enhanced Rainfall for a Cloud Seeding Experiment: Case Studies of Preventing Forest Fire, Drought, and Dust

Yonghun Ro, Ki-Ho Chang, Sanghee Chae, Yun-Kyu Lim, Jung Mo Ku, and Woonseon Jung

Research Applications Department, National Institute of Meteorological Sciences, 33, Seohobuk-ro, Seogwipo-si, Jeju-do 63568, Republic of Korea

Correspondence should be addressed to Ki-Ho Chang; bosupapa@gmail.com

Received 26 December 2022; Revised 17 May 2023; Accepted 10 June 2023; Published 14 July 2023

Academic Editor: Stefano Federico

In this study, a method for verifying the effect of cloud seeding in the case of a mixture of natural and artificial rainfall bands was proposed, and its applicability to each experimental case was evaluated. Water resources that could be secured through cloud seeding were also quantified for the experiments on forest fire prevention, drought mitigation, and dust reduction in 2020. Data on numerical simulations, radar-derived rainfall, rain gauge-derived rainfall, and weather conditions were applied. Areas with seeding and nonseeding effects were classified according to the numerical simulation results and wind system, and enhanced rainfall was determined by comparing the changes in rainfall between the two areas. The amount of water resources was determined by considering the area of the seeding effect and rainfall density. As a result, 1.74 mm (4.75 million tons) of rainfall increased from the experiment on forest fire prevention, 0.84 mm (1.30 million tons) on drought mitigation, and 2.78 mm (24.44 million tons) on dust reduction. Thus, an average rainfall of 1.0 mm could be achieved through the experiment. These results helped verify the pure seeding effect and achieve the experimental purpose.

1. Introduction

Water-related disasters occur frequently worldwide because of climate change, and their damage is rapidly increasing. In some areas, flash floods occur because of heavy rainfall and typhoons, resulting in flood damage, power outages, and landslides [1–5]. In other areas, rainfall does not occur for a long period, resulting in drought problems and large forest fires due to arid climates [6–9]. Therefore, rainfall has been comprehensively investigated to secure available water resources and improve the atmospheric environment [10, 11].

Various methods for rainfall management worldwide have been proposed. For example, the amount of water resources can be increased by storing rainfall on the ground with dams, reservoirs, and rain gutter or by growing cloud droplets. Rainfall storage has been addressed in water resources engineering [12–14], whereas the latter has been conducted through cloud seeding experiments in meteorology [15–17]. Cloud seeding enhances rainfall by seeding hygroscopic materials in clouds to identify the processes of cloud physics.

In China, the United States, Israel, and Japan, cloud seeding has been studied to mitigate drought and suppress hail. Hygroscopic and glaciogenic materials are spread into clouds by using aircraft, rockets, and ground-based cloud seeding generators [18–25]. In most experiments, dry ice, calcium chloride ($CaCl_2$), and silver iodide (AgI) are used to enhance precipitation. These experiments have been performed to prevent forest fires in arid regions, secure visibility in foggy regions, and control typhoon tracks [26–29].

In Korea, since the National Institute of Meteorological Sciences (NIMS) introduced the aircraft in 2017, studies on weather modification have been conducted to mitigate drought, prevent forest fire, dissipate fog, and reduce dust. It

plans to perform a cloud seeding experiment based on numerical simulation (NS) and applies various types of equipment that can observe rainfall and cloud particles to verify the seeding effect on a target area. The NIMS also aims to develop a seeding strategy based on cloud characteristics by securing data from various experiments every year. Thus, research by the NIMS has significantly contributed to the field of cloud physics [30].

Despite these studies, accurately analyzing the changes in the amount of rainfall through cloud seeding experiments is difficult [15, 31–34]. In most studies, seeding effects are determined by statistically analyzing long-term experimental cases. In the United States, Climax I and II experiments conducted to verify the seeding effect on a mountainous terrain in winter from 1960 to 1970 revealed that the rainfall was increased by 18% [35–37]. We reanalyzed this result and made corrections for a 10% increase in rainfall. Recently, Rasmussen et al. [38] statistically analyzed an experiment for 6 years (2008–2013) and confirmed that 1.5% of the enhanced rainfall (ER) can occur in the analysis regions after seeding. In Israel, various cloud seeding experiments were performed from 1961 to 1975 to statistically analyze long-term data; they confirmed that the rainfall was increased by approximately 15% in the northern part of the experimental area [39, 40]. In the United Arab Emirates, Hosari et al. [41] analyzed heavy rainfall events in the years when seeding was not performed (1981–2002) and in the years when seeding was performed (2003–2019); they analyzed and confirmed the annual average of 23% ER in the seeding area. These studies have difficulties securing long-term data; therefore, for rapid technological improvement, an analysis technique for each event is needed despite uncertainties.

A method that can separate the pure rainfall amount from a natural cloud system should be developed to verify the seeding effect in each case. The simplest method is determining the amount of rainfall by comparing the characteristics of the seeding and nonseeding effect areas. Through ER calculation, the usefulness of cloud seeding in securing water resources can be verified. Furthermore, it can be helpful in planning economic and efficient experiments for various purposes, such as forest fire prevention and ecological protection in the future.

In this study, a method for calculating the effect of cloud seeding was developed by classifying the seeding and nonseeding effect areas. Changes in the rainfall system according to seeding materials were confirmed, and the amount of water resources that could be secured through the experiments for each case was calculated.

In Section 2, the characteristics of the data used in this study are summarized. In Section 3, the algorithm proposed for calculating the amount of ER that could be secured through a weather modification experiment is introduced. In Section 4, after the algorithm was applied to the three events in 2020, the seeding effect for each case was quantitatively determined. In Section 5, results are summarized, expected effects are discussed, and directions for future studies are presented.

2. Data

2.1. Rain Gauge-Derived Rainfall and Radar-Derived Rainfall. Rainfall affected by the seeding effect can be observed using ground observation and remote sensing equipment. Rain gauges are used to easily observe rainfall from the ground and record the rainfall intensity at 1-minute intervals. This value represents the average intensity of the rainfall observed during this period. Rainfall data calculated by accumulating this value for a certain period were analyzed in this study. The cumulative time was determined to be within 3–6 h. Rain gauge observation data can easily capture the rainfall characteristics of the target area.

Remote sensing observation data can be used to analyze the characteristics and track the rainfall band affecting the surrounding area. A radar is a device that indicates the intensity of rainfall by analyzing the electrical signal power reflected from the raindrops. In this study, radar-derived rainfall was applied to effectively analyze the seeding effect, which can appear spatially wide. Rainfall was calculated using radar reflectivity, the temporal resolution of the data was 5 min, and the spatial resolution was 1 km × 1 km. Hybrid surface rainfall (HSR) radar reflectivity [42], which is observed at an altitude closest to the ground, was applied to minimize the deviation between the rain gauge- and radar-derived rainfall. Radar-derived rainfall was calculated using the following Z–R relationship, which is used to estimate the spatial distribution of rainfall by the Korea Meteorological Administration (KMA):

$$Z = 148R^{1.59}, \tag{1}$$

where Z is the radar reflectivity (mm^6/m^3) and R is the rainfall (mm/h). Reflectivity is a value indicating the number of water droplets per unit volume. Since the range of observations varies widely, data were stored in units of decibel relative to Z such as 10log (Z). The KMA was used to provide a synthetic rainfall image in real time via equation (1).

2.2. Numerical Simulation for Weather Modification Experiment. The NS results of the effect of the seeding material are required to determine the seeding effect because directly tracking the seeding material diffused into the atmosphere is practically difficult. In addition, numerical models are helpful in determining the optimal experimental area where the seeding effect is expected because the diffusion rate and direction can be initially determined according to the flight area and weather conditions through a preliminary simulation. Considering this advantage, the NIMS determines the target area based on the NS before the experiment [30]. Table 1 summarizes the numerical models in NIMS [43].

The numerical model simulates the cloud growth and extinction process using the Morrison microphysics scheme. The model also utilizes the Yonsei University (YSU) planetary boundary layer scheme, the NOAH land surface scheme, and the MM5 similarity surface layer scheme. In this study, cloud seeding experiments were analyzed using the numerical model with settings shown in Table 1.

Table 1: Numerical model of cloud seeding in NIMS [43].

Period (UTC)	0000–1800
Model top	50 hPa
Longwave radiation	Rapid radiative transfer model (RRTM)
Shortwave radiation	Goddard shortwave scheme
Planetary boundary layer (PBL)	Yonsei University (YSU) scheme
Land surface	NOAH land surface scheme
Surface layer	MM5 similarity
Microphysics	Morrison scheme with glaciogenic/hygroscopic cloud seeding parameterization
Horizontal grid interval	1 km
Initial and boundary condition	Unified model local data assimilation and prediction system (UM LDAPS) analysis data (3 hr, 1.5 km)

Numerical models show that the growth and extinction of rainfall as seeding materials are spatially diffused. Considering this phenomenon, the time when the ER is maximized after seeding can be determined. The effect of natural rainfall in an area with a simulated ER may be checked by using other observational data in the same period. In this study, data from the NS that showed the changes in cumulative rainfall (CR) were used to verify the seeding effect. Changes in the CR indicated an increase or decrease in rainfall in areas expected to be affected by the seeding material. Thus, regions where changes are expected in cloud seeding experiments can be compared. Therefore, the spatial scale of a seeding material in a rainfall system may be determined, consequently allowing the analysis of the seeding effect in an area where a change in rainfall is expected even if it is not a target area.

2.3. Weather and Topography Conditions. When the seeding material is diffused into the target area, it is significantly affected by meteorological factors. The weather conditions in the experimental area should be considered to determine the seeding effect quantitatively. Because the seeding material is spread directly from the aircraft, it is significantly affected by the wind system in the experimental area. The wind direction and velocity influencing diffusion differ depending on the seeding altitude. However, verifying the seeding effect in the target area is difficult if the experiment is not conducted in the planned area because of flight limitations. Even if the aircraft spreads the seeding material at the seeding altitude as planned, rainfall may not occur in the target area, depending on the wind characteristics of the inflow rainfall system. The meteorological data observed from the aircraft after the cloud seeding experiment were analyzed. Weather charts and satellite images were also analyzed to figure out the cloud characteristics. These images show the effect of the low pressure or cold front on clouds with a mixed seeding effect and the cloud distribution near the experimental regions. For the analysis of satellite images, infrared images corresponding to the 8.7 μm wavelength of the GK2A satellite were applied.

One of the meteorological factors to consider along with the wind system at the seeding altitude is temperature. Temperature affects seeding material determination used in the cloud seeding experiment. When the temperature of the seeding altitude is above 0°, $CaCl_2$ is applied; when the temperature is below 0°, AgI spreads to induce the enhancement of ice formation. The updraft rate at the seeding altitude and liquid water content (LWC) also affect experimental results. The stronger the vertical velocity of the cloud in which the seeding material is diffused or the more the LWC, the more favorable the rainfall enhancement. The condition of LWC in the seeded cloud was observed by the aircraft. In addition, the image of P-velocity, which represents the index of vertical velocity, was generated by a very short-range data assimilation and prediction system (VDAPS) for the analysis of temperature and updraft in this study. The intensity of updraft according to the region, the contour line indicating the region with a similar temperature, the relatively cold regions (C) and the warm regions (W), and the wind speed are included in this image.

The impact of topographical factors on the rapid growth of clouds and rainfall bands should be considered. However, interpreting orographic effects on cloud growth is not straightforward [44]. As clouds are more likely grow on a mountainous terrain than in urban areas, orographic effects should be excluded to verify the pure ER by the seeding material. In the case of the mountainous terrain around the target area, rain gauges with a difference of ≥300 m than the average altitude of the observation stations were excluded from the seeding effect analysis in this study.

3. Calculation of the Total Amount of the Enhanced Rainfall

Changes in clouds before and after seeding can be analyzed to verify the seeding effect, and regions affected by the seeding material can be compared with regions not assigned for the same cloud system. In the former case, a cloud can be stagnant or the characteristics do not change significantly over time; therefore, meeting the conditions when conducting the experiment on the Korean Peninsula is difficult. In this study, a method for estimating the amount of rainfall was proposed by comparing the area affected by the seeding material with the neighboring area where clouds with similar characteristics are distributed. This system can classify the seeding and nonseeding effect areas based on the wind system and calculate the total amount of water resources that can be secured through the cloud seeding experiment (Figure 1).

The algorithm consists of four steps (Figure 1): determination of analysis time (AT), determination of seeding effect box (SB) and nonseeding effect box (NB), calculation

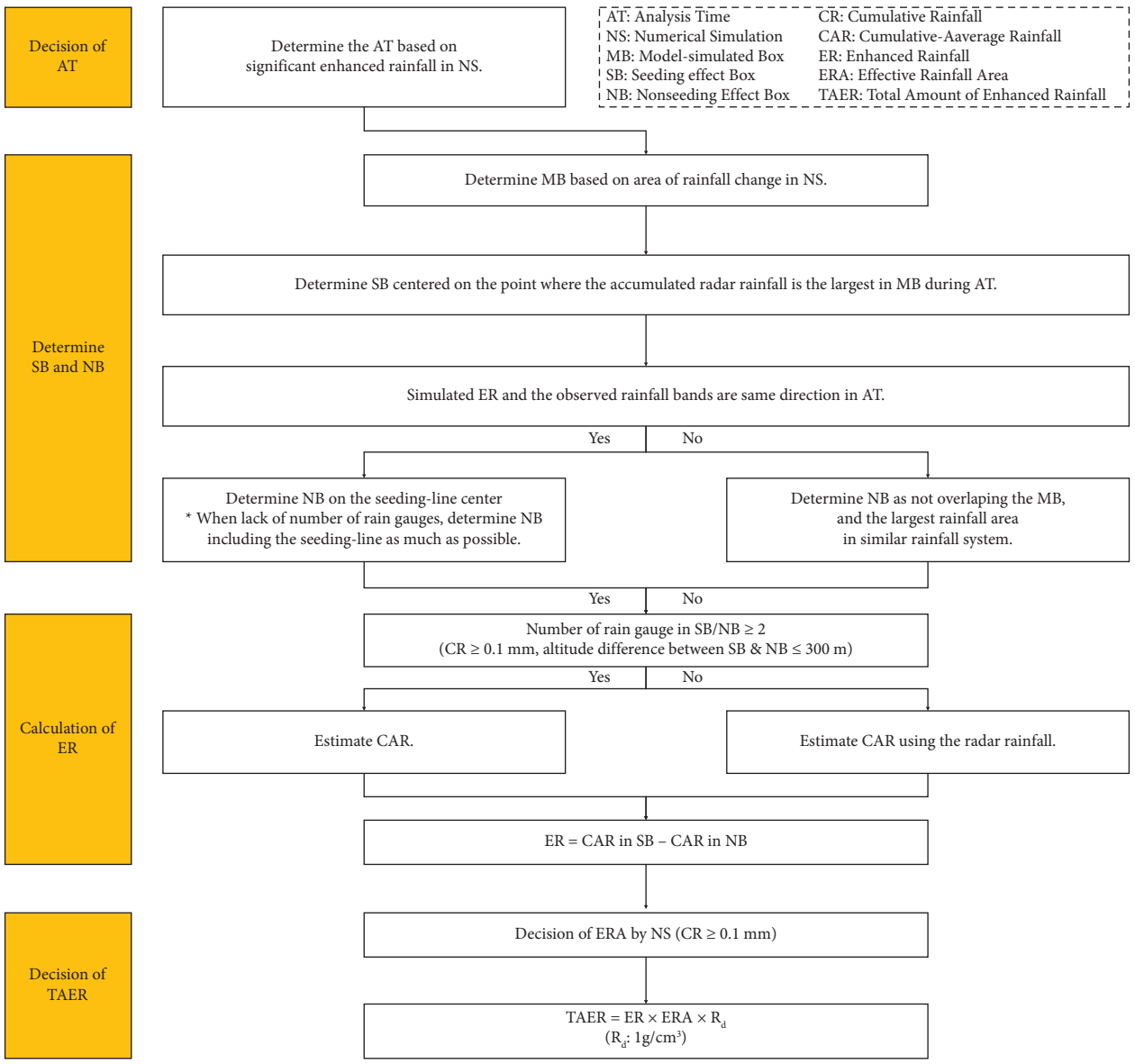

Figure 1: Algorithm for determining the seeding and nonseeding effect areas and estimation of the total amount of enhanced rainfall.

of ER, and determination of the total amount of enhanced rainfall (TAER). In AT determination, the major period when the rainfall changed in the target area according to the diffusion of the seeding material is determined. In this study, AT was identified on the basis of the period of rainfall change near the target area in the NS. In addition, considering that the CR may be excessive depending on the rainfall characteristics flowing into the target area, AT was set to prevent exceeding a maximum of 6 h.

Once AT has been determined, the areas affected and not affected by the seeding material should be classified. First, the area of the major rainfall change during the AT is marked with a red-dotted-line box referred to as a model-simulated box (MB). The seeding-affected area is determined on the basis of the area with the largest radar CR change in the MB. Considering the range in which the effective seeding effect can be verified in the rainfall band, the seeding effect area is determined as a red box (50 km × 50 km) and referred to as the seeding effect box (SB). The nonseeding-affected area is determined as a blue box (50 km × 50 km, such as the SB) according to the wind direction of the ER and natural rainfall band shown in the NS and referred to as the nonseeding effect box (NB). If the two directions are similar, the NB is determined on the basis of the center of the seeding line of the aircraft located on the windward side of the SB. If the rain gauge-derived analysis of the NB is insufficient, the location of the NB can be slightly corrected to include as much of the seeding line as possible. If the direction of the ER in the NS is different from that of the observed rainfall band, the NB is determined on the basis of the area with the greatest rainfall among the same natural rainfall systems without overlapping the MB.

The ER can be calculated by comparing SB and NB. If two or more rain gauges are present where the CR exceeds

0.1 mm during the AT in both areas, the cumulative average rainfall (CAR) of each area is calculated using the observation data. At this time, the altitude of the rain gauges in the NB does not differ by more than 300 m from the average altitude of the rain gauge in the SB. If the CAR is small or missing and if less than two rain gauges are available under the corresponding conditions, the radar-derived CAR estimated at each location of the rain gauge is analyzed. However, considering the estimated rainfall accuracy, the amount of the radar rainfall should be higher than 60% compared to that of the rain gauge rainfall. ER can be calculated as the difference between the CAR of the two areas. This technique is based on assumption that the seeding effect is mixed with the rainfall system flowing into the SB. The calculated value is the average amount of rainfall that can be generated in the area affected by the cloud seeding experiment.

If the estimated area where rainfall may be generated is applied to the calculated ER, the amount of water resources that can be secured through the cloud seeding experiment can be determined. In this study, this parameter was defined as the TAER. The estimated rainfall area was calculated using NS, which is referred to as the effective rainfall area (ERA). The ERA was determined by adding the areas where CR was expected to be 0.1 mm or more during the AT, and only the rainfall area of the land part, excluding the sea, was considered. The TAER can be calculated by multiplying the amount of artificial rainfall, effective rainfall area, and rainfall density for unit conversion, as shown in following equation:

$$\mathrm{TAER} = \mathrm{ER} \times \mathrm{ERA} \times R_d, \tag{2}$$

where the unit of TAER is tons and R_d is the rainfall density assumed to be 1 g/cm^3. The calculated TAER represents the amount of water resources that can be secured through a cloud seeding experiment.

4. Application Examples

4.1. Events and Weather Conditions. In this study, three cases were selected from the cloud seeding experiments performed at NIMS in 2020, and the seeding effect was analyzed. Experimental cases on forest fire prevention, drought mitigation, and dust reduction were selected. Cloud seeding experiments were then performed in different areas according to each purpose. A research aircraft (Beachcraft King Air 350 HW) was used to conduct the experiment. For forest fire prevention, the experiment was conducted in Gangwon-do, and the Cloud Physics Observation Site (CPOS), a verification site for cloud seeding in NIMS, was set as the target area (Event 1). For drought mitigation, the experiment was conducted to increase the storage of Boryeong Dam in Chungnam Province (Event 2). For dust reduction, the experiment was carried out in the capital area, and the KMA observation site located in Seoul (capital) was set as the target area (Event 3). The experimental results of the events and weather conditions observed by the aircraft during the experiment are summarized in Table 2. The analyzed weather map, satellite image, and cloud image of the experimental area are shown in Figure 2.

In Table 2, stratiform clouds were observed in all three experiments conducted at an altitude of approximately 2 km for Events 1 and 2 and less than 1 km for Event 3. $CaCl_2$ was spread as the seeding material because of the temperature higher than 0°C at the seeding altitude. The wind speed in Event 2 was the highest, and the wind direction was affected by the southwest wind in all three cases. The vertical velocity was the same in Events 1 and 2, and Event 3 was the largest among the three cases. The LWC at the seeding altitude was 0.2–0.4 g/m^3 in all three cases, confirming that the experiment was conducted on clouds containing sufficient water droplets. The weather chart in Figure 2 shows that the cloud seeding experiment was performed on clouds affected by a low-pressure front in all the three experiments. Therefore, the cold front passing across the Korean Peninsula after seeding affects the rainfall development. The satellite image shows that Event 1 had thicker clouds than the two other cases. The image taken while seeding from the aircraft confirmed that the experiment was performed in the clouds.

Figure 3 shows the changes in the updraft around the experimental area after seeding. In Table 2, Event 3, which shows a large updraft, can be affected by seeding material diffusion and cloud growth. Figure 3 shows the P-velocity, which represents the index of vertical velocity at the 700 hPa altitude; it was generated by the VDAPS. Considering that the reaction time of the seeding material was different for each event, the figures were shown at intervals of 1 h or 2 h. In Event 1, no significant change was observed in the updraft with time compared with that in the other events, but a strong temperature valley occurred along the east coast. In Event 2, the updraft was weak in the West Sea, but a strong updraft occurred between 14:00 and 15:00 in the center of the inland area. In Event 3, a strong updraft occurred in the northern area at 14:00 as the cold front passed. This updraft influenced the deeper vertical transport of seeding material which affects the enhancement of precipitation.

4.2. Determination of Areas with Seeding Effect and Non-seeding Effect. The NS, rainfall data, and weather conditions were analyzed according to the algorithm shown in Figure 1 to verify the seeding effect in each experimental case. First, AT was determined on the basis of the change in the time of rainfall in the target area. In Event 1, the amount of rainfall after the experiment was not considerably higher than that of the two other cases; therefore, the analysis time was determined to be 6 h from 12:00 to 18:00. In Event 2, the movement speed of the rainfall flowing into the experimental area was relatively fast; thus, the analysis time was 3 h from 13:00 to 16:00 after the experiment. Event 3 was also decided to be 5 h from 13:00 to 18:00 in consideration of the movement velocity of the cloud. Figure 4 shows the time when SB and NB are determined using the results of the ER in the NS and rainfall data from the rain gauge and radar during the AT. Radar-derived rainfall was calculated by applying equation (1) to the HSR reflectivity observed at the rain gauge location.

Table 2: Weather conditions of the three experimental cases.

Event	Date (KST)	Object	Target area	Cloud type	Seeding height (km)	Temperature (°C)	Seeding material	Wind speed (m/s)	Wind direction	Vertical velocity (m/s)	Liquid water contents (g/m^3)
1	2020.03.27 10:59~11:11	A	CPOS	Sc	2.2	3.3	$CaCl_2$	9.0	WSW	0.3	0.21
2	2020.05.15 12:43~13:05	B	BRD	Sc	1.9	10.8	$CaCl_2$	15.0	SW	0.3	0.38
3	2020.11.01 11:26~12:20	C	KMA	St	0.7	6.0	$CaCl_2$	10.0	SW	1.3	0.30

Note: A: forest fire prevention, B: drought mitigation, C: dust reduction, Sc: stratocumulus, St: stratus.

In the analysis result of Event 1 (Figure 4(a)), the cloud seeding experiment was performed in the western part of the CPOS, and the ER appeared widely over the East Sea because of the influence of the southwest wind. The SB was determined to include the eastern part of Gangwon-do and a part of the East Sea, where the major rainfall changes occurred. The SB was determined to include the target area CPOS and the vicinity of Gangneung (GNG), where the radar-derived rainfall was large. Gangneung is a representative coastal city adjacent to the East Sea in central Gangwon-do. The spatial distribution of the radar CR showed that the natural rainfall system moved southeast. This indicates that the wind direction in the coastline was northwest different from that in the seeding effect area due to the mountain ranges. Therefore, because the simulated ER and natural rainfall bands had different directions, the NB was determined in the northern region of the SB without the seeding effect among the regions with similar rainfall clouds to the SB. NB included Sokcho (SOC), a city in the northern part of the East Sea, and the northernmost region in South Korea.

In Event 2, the experiment was conducted over the west sea, southwest of Boryeong Dam (BRD), which is the target area, and the seeding effect was expected diagonally because of the influence of the cold front accompanied by the southeast wind (Figure 4(b)). Although the area of the ER was smaller than that of Event 1, the SB was wider. SB included the Boryeong Dam (BRD) and Gunsan (GSN) areas. Gunsan is an urban area adjacent to the West Sea, near the border between the central and southern regions of South Korea. Because the movement direction of the natural rainfall band appeared to the northeast in the same way as in the direction of the simulated ER, unlike Event 1, NB was determined to include the windward seeding line. Considering that the cloud seeding experiment was performed in the West Sea, the NB was determined to include the analyzed rain gauge and seeding line as much as possible.

The wind system of Event 3 appeared to be in the southwest similar to Event 2; because it was aimed at the KMA station in Seoul, the experiment was conducted in the West Sea (Figure 4(c)). Compared with the two other events, the widest regions were the ones where rainfall changes would occur because of the rapid movement of the cold front. The SB, including the West Sea, the capital area, and Gangwon-do, was determined to be the largest. The SB also included Ansan (ASN), a satellite city located in the northern part of Gyeonggi-do and Seoul, where the radar-derived rainfall was the strongest. NB was determined in the windward seeding line area as in Event 2, considering that the wind direction of the rainfall system and the simulated ER are the same.

Table 3 summarizes the basic information of the analyzed rain gauge included in each box determined by the event. In addition to the location of the rain gauge, the altitude from the sea level and the CR of the rain gauge and radar during the AT are shown in Table 3. In Event 1, data from rain gauges distributed near the shoreline were analyzed in NB and SB to exclude the orographic effect on the rainfall cloud. Therefore, seven stations, including Gangneung (GNG), were selected for SB and four stations, including Sokcho (SOC), were chosen for NB. In Event 2, SB had 15 stations, including Boryeong Dam (BRD) and Gunsan (GSN), and NB had 6 stations. At Daecheonhang (DCH) in the SB and Galmaeyeo (GMY) in the NB, no rainfall was observed during the AT. In Event 3, in Figure 4(c), only stations with an elevation of less than 100 m above sea level were analyzed considering the excessive concentration of rain gauges around the capital area. Accordingly, 25 stations, including the KMA, were selected in the SB, and 5 stations were chosen for the NB. At the GDA station in the NB, no rainfall was observed in the AT.

In Table 3, the CR during AT was greater on the rain gauge than on the radar. At the SHA station in Event 3, the rain gauge-observed rainfall was at least three times greater than the radar-derived rainfall because the rainfall observation methods of rain gauge and radar are different; furthermore, rain gauge rainfall observations can be significantly influenced by the surrounding weather condition. Although radar-derived rainfall may have a lower measurement accuracy than rain gauge-derived rainfall, radar rainfall is advantageous for analyzing the average characteristics of rainfall systems distributed in the atmosphere. Therefore, in this study, the changes in the radar average reflectivity before and after seeding in the two areas were compared (Figure 5).

In all three events, the increasing and decreasing trends of the average reflectivity of SB were similar to those of NB (Figure 5). The locations of the two regions were different, and the time of increase in reflectivity did not coincide because clouds affected the SB after they passed through the

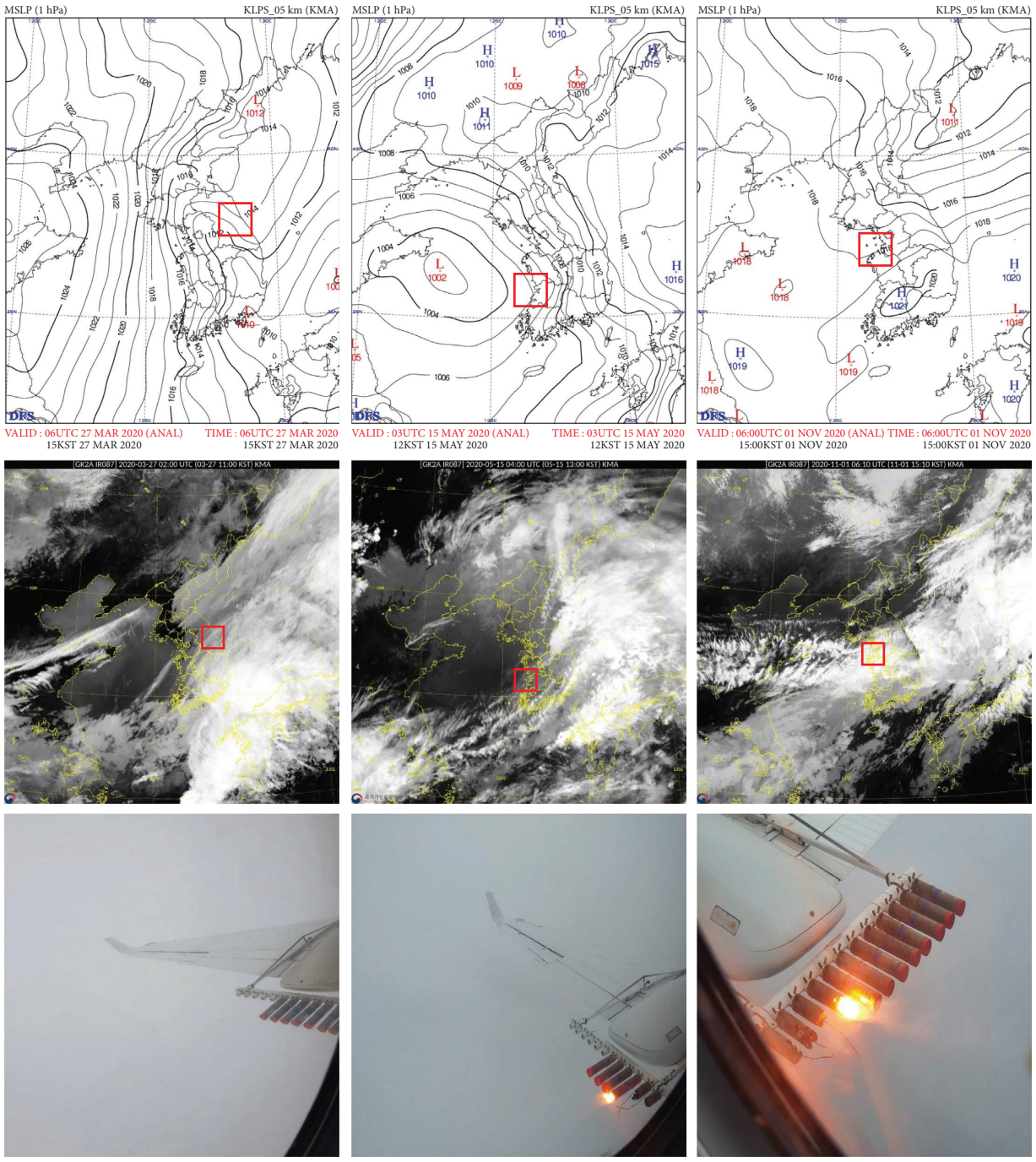

FIGURE 2: Images of weather charts, cloud by satellite, and aircraft seeding for the three experimental cases. The red box includes the experimental area for each case. The contours in weather charts represent atmospheric pressure (hPa). The cloud images were generated from infrared image (8.7 μm) in GK2A satellite. (a) Event 1. (b) Event 2. (c) Event 3.

NB in all three events; however, this trend showed that the cloud characteristics observed in the two regions were similar. In Event 1, radar reflectivity was continuously observed in both areas before and after seeding. During the AT, the reflectivity increased twice in the SB (13:00–14:05 and 14.13–18.80 dBZ and 14:35–15:20 and 15.24–20.83 dBZ). In the NB, the reflectivity increased at a similar time (13:00–14:10 and 13.91–17.97 dBZ and 14:40–15:10 and 12.79–14.96 dBZ), that is, reflectivity increases in the two intervals are 4.67 and 5.59 dBZ in SB and 4.06 dBZ and 2.17 dBZ in NB. If the cloud characteristics of the two regions were similar, the reflectivity was increased by 0.61–3.42 dBZ because of the effect of the seeding material in Event 1.

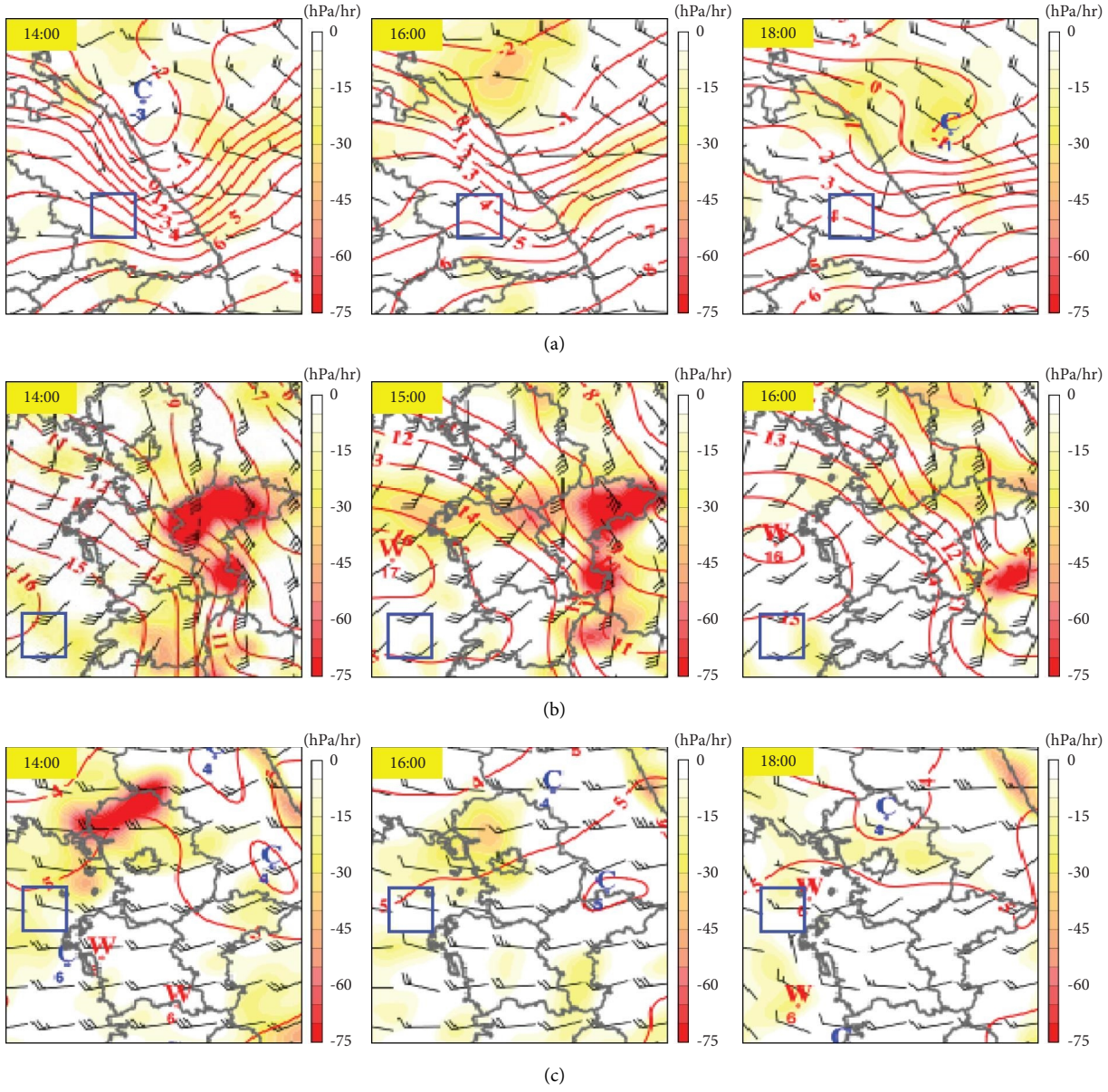

Figure 3: Comparison of VDAPS updraft at a 700 hPa altitude for the three experimental cases. The contours indicate temperature, and *W* and *C* represent relatively warm and cold state at such altitude. The shadings represent intensity of updraft (hPa/hr). The blue box includes the experimental area for each case. (a) Event 1. (b) Event 2. (c) Event 3.

In Event 2, the radar reflectivity in both areas decreased. In the SB, reflectivity was continuously observed; in the NB, it was observed until 15:30 only. At the time of analysis, reflectivity decreased in the SB, but it temporarily increased by 5.02 dBZ from 8.81 dBZ to 13.83 dBZ at 14:25–14:55. This relative increase is not well apparent from Figure 5(b) in the written time range. Presently, it is not scientifically clear how to distinguish between natural rainfall and cloud 332 seeding-induced rainfall [21]. However, in Figure 5(b), the average reflectivity of the effective time (green-shaded box) is 13.8 dBZ in the SB and 13.1 dBZ in the NB though it is an indirect verification.

In Event 3, reflectivity was observed only before 17:00 in both areas. Unlike the two other events, the reflectivity between the two areas before the AT largely differed but showed similar increasing and decreasing trends during the AT. This finding showed that the characteristics of rainfall flowing into the two regions changed consistently (homogeneously) over time. In the AT, as in Event 1, a two-fold increase in radar reflectivity was observed because of the effect of the seeding material. In the NB, reflectivity changed significantly over time. Therefore, rainfall in both the areas should be analyzed to verify the seeding effect. Figure 5 illustrate that the seeding effect can be verified using rain gauge-measured data.

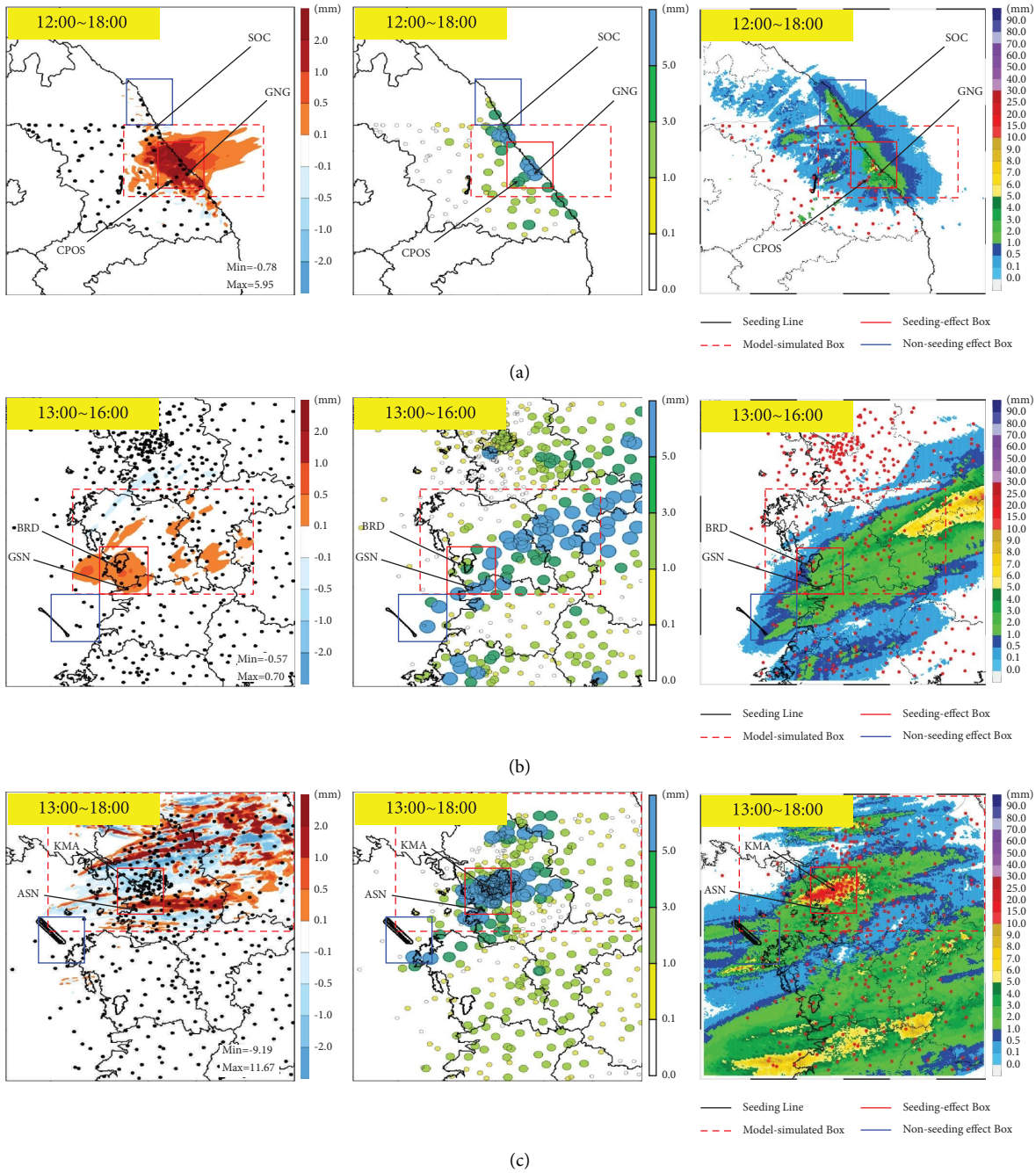

FIGURE 4: Determination of the model-simulated box (red-dotted), the seeding effect box (red), and the nonseeding effect box (blue) for the three experimental cases. From left to right: numerical simulation for enhanced rainfall, rain gauge-derived rainfall, and radar-derived rainfall. The black line represents the seeding line. (a) Event 1. (b) Event 2. (c) Event 3.

4.3. Determination of the TAER. Once the SB and NB are determined, the amount of ER can be calculated according to Figure 1. The CAR of the two areas can be determined and the ER can be calculated using the rain gauge- and radar-derived rainfall data shown in Table 3. Table 4 shows the statistical data of the CR of the rain gauge- and radar-derived data in each box by event and the amount of ER calculated by the difference in average rainfall between the two areas.

In Table 4, rain gauge- and radar-derived rainfall is statistically analyzed using only the data observed for the CR of ≥0.1 mm (Figure 1). As shown in Table 4, the CAR of the radar was smaller than that of the rain gauge. The maximum value and variance of radar rainfall were also smaller than those of rain gauge rainfall except in Event 1. In the NB of Event 1, the variance of the radar-derived rainfall was the smallest among all cases. In rain gauge-derived rainfall, the variance was the largest in the SB of Event 3 among all cases.

Table 3: Basic information of rain gauges in seeding effect box and nonseeding effect box.

Case	Seeded area						Nonseeded area					
	Station	Lat	Lon	Height (m)	Gauge (mm)	Radar (mm)	Station	Lat	Lon	Height (m)	Gauge (mm)	Radar (mm)
27 Mar 2020	BGN	37.805	128.855	75.2	5.60	7.30	SOC	38.251	128.565	17.5	3.60	2.31
	GNG	37.752	128.891	27.1	5.60	3.27	GSG	38.385	128.475	6.1	3.50	1.86
	JMJ	37.899	128.821	8.9	4.00	4.68	DJN	38.492	128.428	21.5	2.50	1.87
	GAM	37.786	128.925	6.6	2.50	3.07	HNE	38.544	128.403	5.5	1.00	2.02
	YGO	37.852	128.819	8.4	5.50	3.86						
	OGE	37.614	129.029	58.4	3.50	1.07						
	YAY	38.087	128.630	4.3	4.00	2.67						
15 May 2020	GSN	36.005	126.761	27.9	6.80	3.07	MDO	35.858	126.315	44.2	3.50	0.60
	BRG	36.327	126.557	10.0	0.50	0.13	SNH	35.442	126.488	16.1	0.50	0.12
	BYE	36.272	126.921	13.4	6.90	2.22	BSN	35.621	126.478	1.9	2.00	1.73
	SCN	36.063	126.704	9.6	3.00	1.56	SYD	35.812	126.398	11.5	5.50	1.46
	CYA	36.424	126.779	98.8	3.50	0.66	WDO	35.602	126.282	4.2	6.00	0.82
	YNH	36.132	126.860	10.7	3.50	1.71	GMY	35.613	126.245	15.0	—	0.55
	CJD	36.174	126.529	7.7	1.50	0.87						
	DCH	36.324	126.502	31.7	0.00	0.15						
	JSN	36.386	126.957	23.8	9.00	1.26						
	HLA	36.046	126.892	49.1	7.00	2.40						
	GSSD	35.950	126.591	5.8	7.00	2.01						
	BRD	36.247	126.633	80.0	2.00	1.23						
	DHD	36.286	126.680	60.0	3.00	1.05						
	MSC	36.289	126.678	85.6	3.00	1.05						
	MSM	36.211	126.678	89.5	4.00	1.57						
1 Nov 2020	BDG	37.383	127.119	55.7	2.00	2.52	TAN	36.759	126.296	41.9	6.50	5.07
	SHD	37.406	126.784	16.9	12.00	8.81	MLP	36.768	126.121	10.0	8.50	4.71
	KMA	37.494	126.918	44.0	12.00	13.09	SBD	37.171	126.297	10.2	1.76	10.2
	GPJG	37.643	126.673	10.5	1.00	1.22	ADO	36.959	126.168	32.5	0.50	1.50
	SGO	37.746	127.074	53.0	1.50	1.54	GDA	36.770	125.977	16.0	—	1.97
	BCN	37.498	126.767	15.7	13.50	11.79						
	AYA	37.392	126.959	96.0	7.50	4.43						
	GJN	37.324	126.821	73.0	3.50	3.86						
	GMG	37.476	126.866	52.7	16.00	12.87						
	GPO	37.359	126.937	84.7	5.50	5.20						
	GMP	37.647	126.705	28.0	2.00	2.31						
	JGO	37.656	126.833	45.3	2.00	2.62						
	SHA	37.44	126.898	37.0	24.00	7.67						
	HOD	37.422	126.858	36.4	9.50	9.28						
	GCN	37.748	126.777	12.9	0.50	0.80						
	GCD	37.555	126.69	47.0	4.50	3.56						
	ICYS	37.397	126.662	8.1	12.00	8.65						
	EJB	37.735	127.073	89.5	2.00	2.52						
	GYG	37.637	126.892	44.7	3.00	3.88						
	ASN	37.281	126.838	5.9	1.50	2.96						
	SHG	37.392	126.778	5.8	11.00	8.95						
	SNM	37.421	127.125	28.7	6.50	4.55						
	NGK	37.702	126.79	59.1	2.00	1.49						
	GAC	37.44	127.002	46.6	9.00	6.86						
	BPG	37.472	126.751	25.9	18.00	14.42						

These results showed that radar-derived rainfall has a smaller spatial deviation than rain gauge-derived rainfall [45]; however, the amount of rainfall is small [46, 47] because the radar observes raindrops in the atmosphere, but as droplets fall, observation loss may occur in the rain gauge depending on weather conditions. The amount of ER calculated using the difference in CAR between the two boxes was similar to that of the radar and rain gauge. This finding indicated that the observed values might differ at individual points; however, the cloud characteristics distributed in the two areas were similar (Figure 5).

Of course, the ER calculated by this analysis method may vary depending on the location of the area. The SB is determined based on the numerical simulation, but the NB is determined among regions where similar systems are distributed, so it cannot be an objective. Therefore, it is necessary to analyze the sensitivity of the CAR determined according to the location of the NB. In this study, as shown

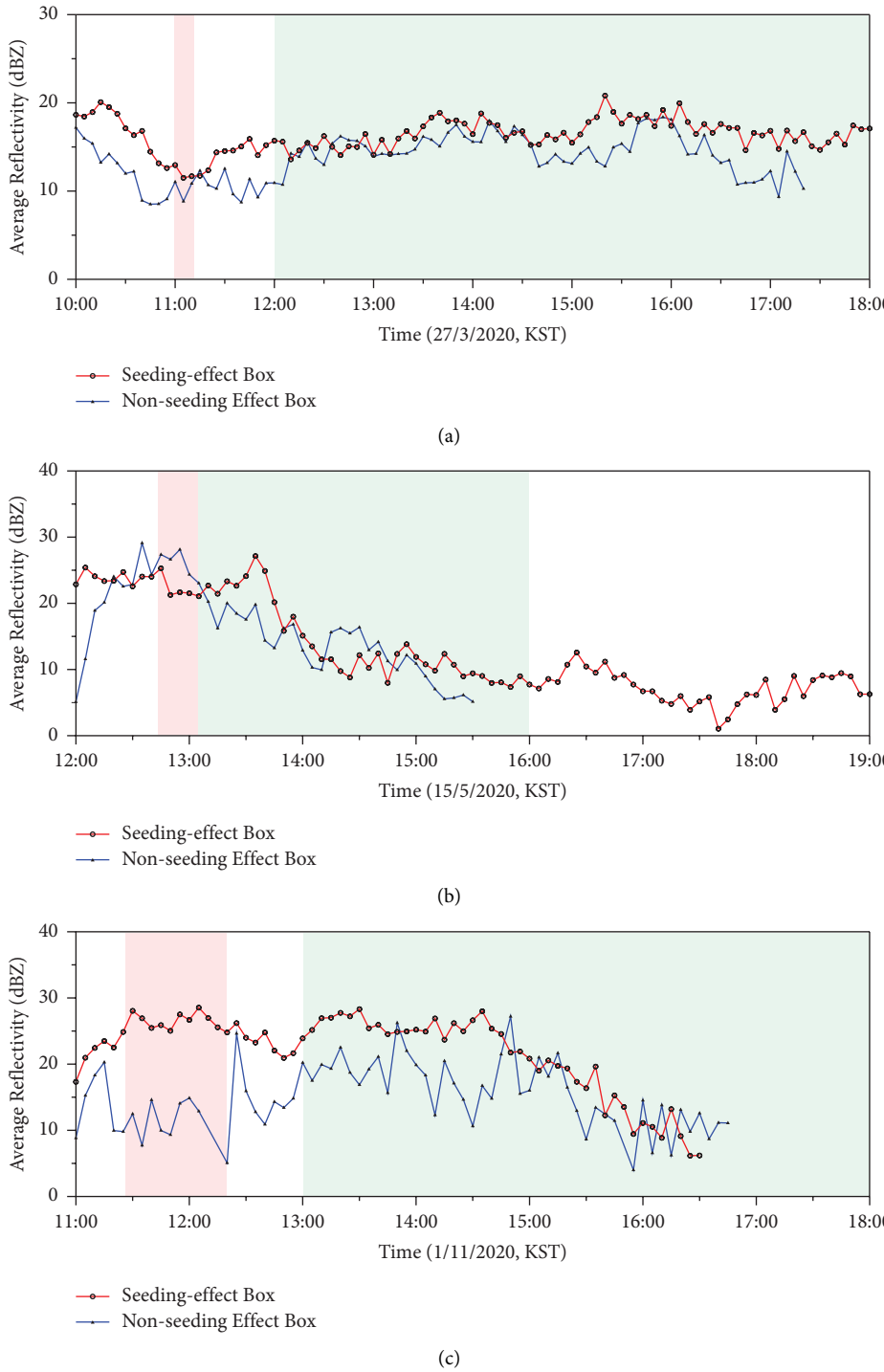

FIGURE 5: Comparison of the average radar reflectivity in the seeding and nonseeding effect boxes for the three experimental cases. The red-shaded box indicates the seeding time and the green-shaded box represents the analysis time. (a) Event 1. (b): Event 2. (c) Event 3.

in Figure 6, the results of the sensitivity analysis are shown for each event. Here, the CAR that changes when the NB in Figure 4 is moved in all directions is compared. The movement directions were considered as southwest, south, southeast, west, east, northwest, north, and northeast based on the NB location in Figure 4 (Basic). In addition, the movement range was set to 25 km, which corresponds to half the size of NB, so that the analysis rain gauge could be changed without overlapping with the SB as much as possible.

In Figure 6(a), showing the result of Event 1, the CAR of the rain gauge in the NB determined by the algorithm was medium compared to that calculated in other locations. Rainfall increased as the unaffected area moved

Table 4: The basic statistics of cumulative rainfall for the seeding effect box and nonseeding effect box and calculated enhanced rainfall in seeding effect area.

Event			Cumulative rainfall		Enhanced rainfall in seeding effect area (mm)
			Seeding effect box	Nonseeding effect box	
1	Rain gauge	Maximum (mm)	5.60	3.60	1.74
		Mean (mm)	4.39	2.65	
		Variance (mm^2)	1.47	1.46	
	Radar	Maximum (mm)	7.30	2.31	1.68
		Mean (mm)	3.70	2.02	
		Variance (mm^2)	3.75	0.04	
2	Rain gauge	Maximum (mm)	9.00	6.00	0.84
		Mean (mm)	4.34	3.50	
		Variance (mm^2)	6.44	5.38	
	Radar	Maximum (mm)	3.07	1.73	0.52
		Mean (mm)	1.40	0.88	
		Variance (mm^2)	0.66	0.37	
3	Rain gauge	Maximum (mm)	24.00	8.50	2.78
		Mean (mm)	7.28	4.50	
		Variance (mm^2)	38.90	13.33	
	Radar	Maximum (mm)	14.42	5.07	2.83
		Mean (mm)	5.83	3.00	
		Variance (mm^2)	17.00	3.01	

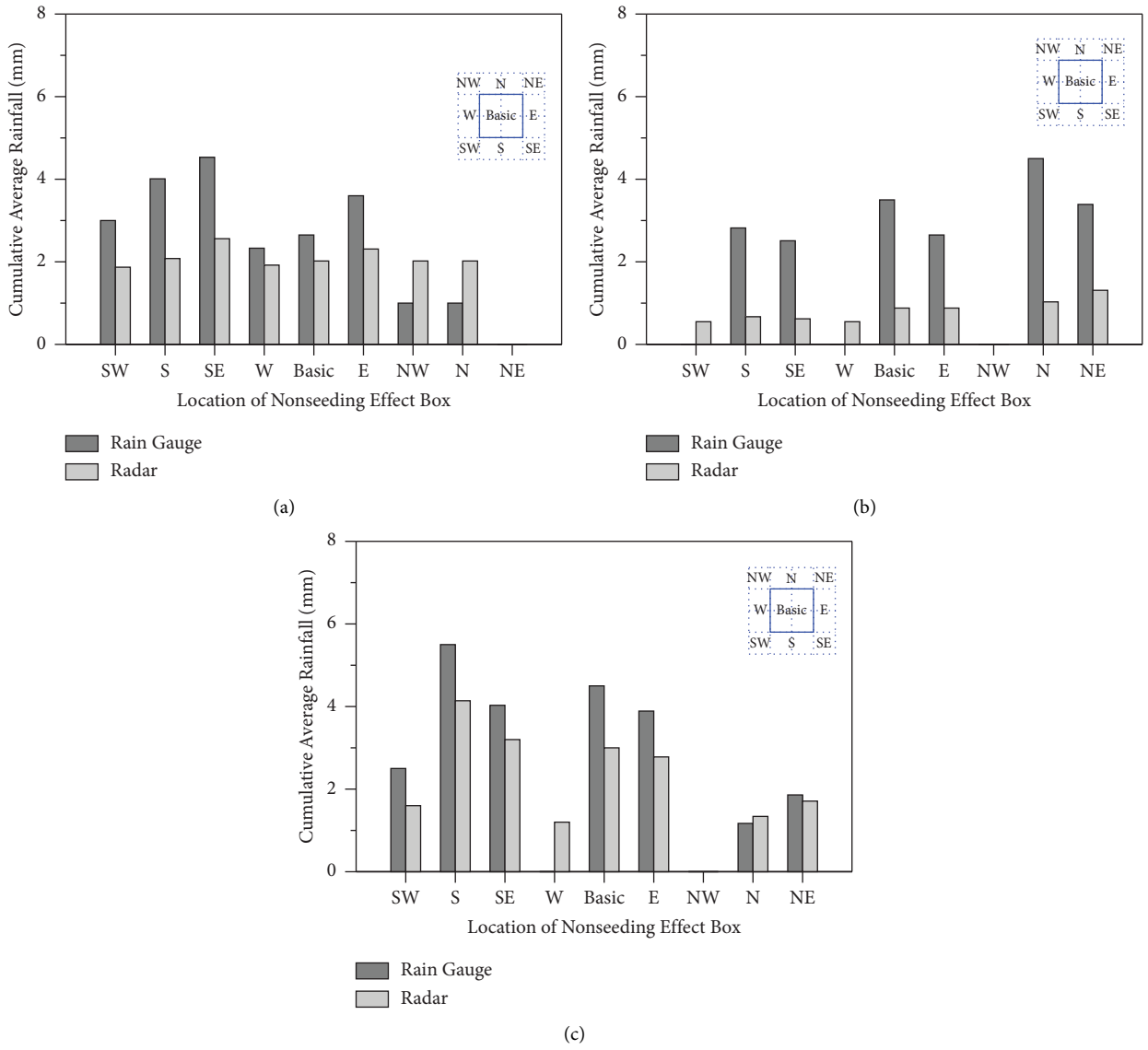

Figure 6: Change of cumulative average rainfall for the rain gauge and the radar according to location of the nonseeding effect box. (a) Event 1. (b) Event 2. (c) Event 3.

Table 5: Calculation of the total amount of enhanced rainfall in the seeding effect area.

Event	Enhanced rainfall in seeding effect area (mm)	Effective rainfall area (km^2)	Total amount of enhanced rainfall (ton)
1	1.74	2,731	4,751,940
2	0.84	1,549	1,301,160
3	2.78	8,793	24,444,540

south and decreased as it moved north. As shown in Figure 4, this is because precipitation was stronger in the southern area of the NB. In addition, since rain gauges are rarely distributed in the northern area, the CR was affected by the small observed value, and when the NB moved northeast, the rain gauges were not included. In the case of the radar rainfall, it was found that the CAR did not change significantly because the precipitation system variation was not large around the NB.

In Events 2 and 3, the CAR of the rain gauge and the radar before the location of the NB was moved which was almost larger than when it was moved to another location (Figures 6(b)-6(c)). In the case of Event 2, when the location of the NB was moved to the west (southwest, west, and northwest), the CAR was not observed due to rarely distributed rain gauge on the sea and no precipitation detection. On the other hand, when the NB was moved inland where the rain gauges are densely distributed, the CAR was

Table 6: Summary of the major results of the total experiments, 2020.

Object	Date	Seeding material	Enhanced rainfall in seeding effect area (mm)	Effective rainfall area (km^2)	Total amount of enhanced rainfall (ton)	Remarks
A	2020.01.29 (12:18~12:27)	AgI	0.16	547	87, 520	Event 1 in this study
	2020.01.30 (11:58~12:09)	AgI	1.11	2,002	2, 222, 220	
	2020.03.27 (10:59~11:11)	$CaCl_2$	1.74	2,731	4, 751, 940	
	2020.04.27 (13:51~14:10)	AgI	0.19	5	950	
	2020.09.25 (09:54~10:32)	$CaCl_2$	0.94	878	825, 320	
	2020.11.19 (11:11~11:30)	$CaCl_2$	3.49	6,344	22, 140, 560	
B	2020.05.09 (11:10~11:26)	$CaCl_2$	0.48	4, 890	2, 347, 200	Event 2 in this study
	2020.05.15 (12:43~13:05)	$CaCl_2$	0.84	1, 549	1, 301, 160	
C	2020.01.06 (16:42~17:07)	AgI	0.20	229	45, 800	Event 3 in this study
	2020.11.01 (11:26~12:20)	$CaCl_2$	2.78	8, 793	24, 444, 540	
	2020.11.01 (15:33~16:29)	$CaCl_2$	0.26	7, 602	1, 976, 520	

calculated to be larger. In Event 3, the rain rate was strong both in the capital area and in the sea, but the CAR was calculated to be large when moving the NB to the inland, where there are many rain gauges. The radar rainfall also showed similar results to the rain gauge rainfall in both cases, but the change in the CAR according to the location of the NB was larger in Event 3 than in Event 2.

Comparing the analysis results, Event 1 showed an ideal result that was close to the median value among the amount for which the CAR could be calculated, and the other two cases had a relatively large CR. However, the amount of the ER calculated in this study is a value calculated by comparing the area affected by seeding with the area on the windward side. If another area is determined for the NB, an ideal result can be obtained, but comparing the seeding-affected area with the nonwindward area is not reasonable for the ER calculation. Therefore, the results of this study were relatively evaluated as the objective CAR in the NB necessary for seeding effect analysis. Based on this sensitivity analysis result, the ER was calculated using ground measurement data assumed to be a true value according to the algorithm shown in Figure 1, in this study. Table 5 shows the calculated ER for each case and TAER calculated by considering the ERA.

In Event 3, the ER was 2.78 mm, which was the largest among the three events and 38.2% compared with that in the SB (Table 5). In Event 2, the ER was the smallest at 0.84 mm (19.4% compared with that in the SB); in Event 1, the ER was 1.74 mm (39.6% compared with that in the SB). These results showed that the pure seeding effect can be separated when natural and artificial rainfall is mixed. The ERA was also estimated in terms of the amount of ER; in particular, in Event 3, rainfall occurred in a larger area than in other cases (Figure 4). As a result, a large amount of water resources could be secured: 4.75 million tons for forest fire prevention, 1.30 million tons for drought mitigation, and 24.44 million tons for dust reduction. These findings were significant because the seeding effect was quantitatively determined for each event. In addition, the expected amount of water resources can help achieve the experimental purposes. In Event 1, the risk of forest fires in dry areas could be lowered by increasing the humidity around the target area. In Event 2, preparations for drought could be made by increasing the amount of water stored in the Boryeong Dam basin. The Boryeong Dam supplied an average of 200,000 tons of water per day as of 2020, and the amount that could be secured through the experiment was equivalent to approximately a week of water supply. The water resources secured in Event 3 could be expected to reduce the concentration of dust in the capital area. Although fundamentally solving drought, forest fire, and dust is difficult, these results are significant because we can secure usable water resources to prepare for disasters through cloud seeding experiments. The analysis results of 20 cloud seeding experiments performed in 2020 in Korea and the experiments corresponding to the three events analyzed in this study are presented in Table 6 as a reference in this study.

Eleven experiments were performed in 2020 (Table 6): six for forest fire prevention, two for drought mitigation, and three for dust reduction. Forest fire prevention experiments were conducted relatively frequently except during the rainy season (June to August) in summer. The drought mitigation experiment was conducted in May, and the dust reduction experiment was performed in January and November. This finding shows that the risk of forest fires and droughts was frequently observed in 2020 because of the dry climate, and dust problems in autumn were significant. If the events were classified according to the seeding material, four experiments for AgI and seven for $CaCl_2$ were performed. In the drought mitigation experiment, AgI was not used because the experiments were conducted in spring when temperature was high.

The amount of ER was at least 0.16 mm (January 29, 2020) to 3.49 mm (January 19, 2020) among the 11 experiments. The ERA varied according to the NS of each case, and the TAER was determined according to the amount of the ER and the size of the ERA. For the minimum rainfall area (April 27, 2020), the total rainfall was as low as 950 tons. For the TAER, Event 3 showed the largest volume of all cases. The ER for 11 cases was a total of 12.19 mm, confirming that an average of at least 1.0 mm of rainfall could be enhanced in one experiment. This analysis result was significant because it could quantitatively verify the effect of cloud seeding in the NS by using the ground measurement data. Fundamentally, it helps achieve experimental purposes by securing domestic water resources in Korea.

5. Conclusions

In this study, a method for verifying the effect of cloud seeding by analyzing the seeding effect and nonseeding effect areas was developed, and its applicability was evaluated. Numerical models, radar and rain gauge-derived rainfall data, and weather condition data were applied. After the seeding effect and nonseeding effect areas based on the numerical data and wind system of rainfall in the target area were determined, the amount of rainfall that increased in the seeding effect area was calculated. The amount of water resources that could be secured through the experiment was also determined in this study. The major results were summarized as follows:

(1) The new analysis method consists of four steps (determination of AT, SB, NB, ER, and TAER). The AT was determined on the basis of the change in the period of rainfall in the target area as shown in the NS. SB was determined to be centered on the area where the radar-derived rainfall was large in the area with the major change in rainfall of the NS. NB was determined according to the consistency of the simulated EP and observed rainfall bands. When the two directions coincided, the seeding line was included as much as possible in the NB. The ER was calculated by comparing the characteristics of the two areas, and the final TAER was determined by considering the ERA and rainfall density.

(2) Three experimental cases were selected to prevent forest fire, mitigate drought, and reduce dust, and SB and NB were determined on the basis of the wind system to verify the seeding effect. In Events 2 and 3, because the wind direction of rainfall was identical to that of the ER, SB was determined in the area with a strong radar-derived rainfall, and NB was

determined at the windward seeding line. Conversely, in Event 1, because the directions of the simulated rainfall and natural system were different, the NB was determined in the area where a similar cloud was distributed. The rain gauges distributed near the coastline were analyzed to exclude orographic effects. During AT, the CR was observed to be greater on the rain gauge than on the radar, and the characteristics of clouds distributed in the two areas were confirmed to be similar.

(3) The amount of ER was calculated for each case by comparing the rainfall in SB and NB, and the amount of water resources that could be secured through the experiment was determined. In Event 1, 1.74 mm of rainfall (4.75 million tons) was generated to prevent forest fires. Furthermore, 0.84 mm (1.30 million tons) for drought mitigation in Event 2 and 2.78 mm (24.44 million tons) for dust reduction in Event 3 were secured. Therefore, an average of 1.0 mm of ER could be secured through the experiments in Korea.

These results showed that the amount of ER was calculated for each case. However, data analyzed with a rain gauge varies depending on the SB and NB locations, an error might occur in ER calculation. Since this study determined the area with the high rain rate as the affected area under the assumption that seeding material is totally converted to artificial rainfall, there is clearly room for error to be reflected in the analysis results if enhanced rainfall does not occur. Therefore, in this study, the change in rainfall according to the location of the NB was compared through sensitivity analysis, and the calculated rainfall was evaluated as objective. Together, numerical model uncertainty could also affect the analysis results; therefore, SB was determined on the basis of the change in radar-derived rainfall in this study. A numerical model verified in previous studies on cloud seeding in Korea [43, 48] was used. In addition, the statistical analysis of long-term experimental cases, such as the existing method, can reduce the error in the calculation of the seeding effect, but a case-by-case analysis method is needed for rapid technological development. More scientific improvement is possible for the next plan by immediately performing an analysis after the experiment.

The results of this study are significant because they can verify the pure seeding effect by isolating natural rainfall from the clouds affected by the seeding material. Of course, since the method of this study cannot completely remove natural variation of precipitation, additional case analysis is required. However, the result of this study is significant because it can determine the seeding effect on a case-by-case compared to previous studies. In the short term, the forecasting performance of the numerical model can be verified; in the long term, water resources should be supplemented through cloud seeding, and the damage caused by forest fires, droughts, and dust must be reduced.

In the future, this study will be used in research fields such as cloud microphysics processes, optimal experimental strategical planning, and improvement of the forecasting performance of numerical models. Furthermore, the results of this study are the effect of an experiment using one aircraft; therefore, increasing the seeding materials or applying several aircraft should be considered to obtain more water resources. Additional ground observation networks and various experimental cases should also be secured to determine the quantitative seeding effect.

Data Availability

The data that support the findings of this study are available from the corresponding author from NIMS, KMA, Korea.

Conflicts of Interest

The authors declare that they have no conflicts of interest.

Acknowledgments

This work was funded by the Korea Meteorological Administration Research and Development Program "Research on Weather Modification and Cloud Physics" under Grant no. KMA2018-00224. The authors would also like to thank for the collaboration with Dr. Tae-Kook Kim and Dr. Sumin Woo in Water Resources Operation Department of Korea Water Resources Corporation (K-water).

References

[1] B. K. Smith and J. A. Smith, "The flashiest watersheds in the contiguous United States," *Journal of Hydrometeorology*, vol. 16, no. 6, pp. 2365–2381, 2015.

[2] S. Mahmood, A. U. H. Khan, and S. Ullah, "Assessment of 2010 flash flood causes and associated damages in Dir Valley, Khyber Pakhtunkhwa Pakistan," *International Journal of Disaster Risk Reduction*, vol. 16, pp. 215–223, 2016.

[3] A. M. S. Pradhan, H. S. Kang, J. S. Lee, and Y. T. Kim, "An ensemble landslide hazard model incorporating rainfall threshold for Mt. Umyeon, South Korea," *Bulletin of Engineering Geology and the Environment*, vol. 78, no. 1, pp. 131–146, 2019.

[4] A. Alipour, A. Ahmadalipour, P. Abbaszadeh, and H. Moradkhani, "Leveraging machine learning for predicting flash flood damage in the Southeast US," *Environmental Research Letters*, vol. 15, no. 2, Article ID 24011, 2020.

[5] M. Kefi, B. K. Mishra, Y. Masago, and K. Fukushi, "Analysis of flood damage and influencing factors in urban catchments: case studies in Manila, Philippines, and Jakarta, Indonesia," *Natural Hazards*, vol. 104, no. 3, pp. 2461–2487, 2020.

[6] D. M. Staley, J. E. Gartner, G. M. Smoczyk, and R. R. Reeves, *Emergency Assessment of post-fire Debris-Flow Hazards for the 2013 Mountain Fire, Southern California*, Geological Survey, Reston, VA, USA, 2013.

[7] M. Z. Xiao, Q. Zhang, V. P. Singh, and L. Liu, "Transitional properties of droughts and related impacts of climate indices in the Pearl River basin, China," *Journal of Hydrology*, vol. 534, pp. 397–406, 2016.

[8] S. Z. Huang, L. Wang, H. Wang et al., "Spatio-temporal characteristics of drought structure across China using an integrated drought index," *Agricultural Water Management*, vol. 218, pp. 182–192, 2019.

[9] A. F. Prein, J. Coen, and A. Jaye, "The character and changing frequency of extreme California fire weather," *Journal of*

Geophysical Research: Atmospheres, vol. 127, no. 9, pp. 1–19, 2022.

[10] K. M. Lau and K. M. Kim, "Observational relationships between aerosol and Asian monsoon rainfall, and circulation," *Geophysical Research Letters*, vol. 33, no. 21, pp. L21810–L21815, 2006.

[11] M. Falkenmark and J. Rockström, "Building resilience to drought in desertification-prone savannas in Sub-Saharan Africa: the water perspective," *Natural Resources Forum*, vol. 32, no. 2, pp. 93–102, 2008.

[12] K. S. Chartzoulakis, N. V. Paranychianakis, and A. N. Angelakis, "Water resources management in the island of Crete, Greece, with emphasis on the agricultural use," *Water Policy*, vol. 3, no. 3, pp. 193–205, 2001.

[13] S. Dessai and M. Hulme, "Assessing the robustness of adaptation decisions to climate change uncertainties: a case study on water resources management in the East of England," *Global Environmental Change*, vol. 17, no. 1, pp. 59–72, 2007.

[14] H. Furumai, "Rainwater and reclaimed wastewater for sustainable urban water use," *Physics and Chemistry of the Earth, Parts A/B/C*, vol. 33, no. 5, pp. 340–346, 2008.

[15] B. Geerts, Q. Miao, Y. Yang, R. Rasmussen, and D. Breed, "An airborne profiling radar study of the impact of glaciogenic cloud seeding on snowfall from winter orographic clouds," *Journal of the Atmospheric Sciences*, vol. 67, no. 10, pp. 3286–3302, 2010.

[16] S. A. Tessendorf, R. T. Bruintjes, C. Weeks et al., "The Queensland cloud seeding research program," *Bulletin of the American Meteorological Society*, vol. 93, no. 1, pp. 75–90, 2012.

[17] R. M. Rauber, B. Geerts, L. Xue et al., "Wintertime orographic cloud seeding-a review," *Journal of Applied Meteorology and Climatology*, vol. 58, no. 10, pp. 2117–2140, 2019.

[18] V. J. Schaefer, "The production of ice crystals in a cloud of supercooled water droplets," *Science*, vol. 104, no. 2707, pp. 457–459, 1946.

[19] E. B. Kraus and P. Squires, "Experiments on the stimulation of clouds to produce rain," *Nature*, vol. 159, no. 4041, pp. 489–491, 1947.

[20] D. W. Reynolds, "Design of a ground based snowpack enhancement program using liquid propane," *Journal of Weather Modification*, vol. 21, no. 1, pp. 29–34, 1989.

[21] R. T. Bruintjes, "A review of cloud seeding experiments to enhance precipitation and some new prospects," *Bulletin of the American Meteorological Society*, vol. 80, no. 5, pp. 805–820, 1999.

[22] S. Javanmard, J. BodaghJamali, and A. M. Noorian, "Preliminary results of site selection study for cloud seeding in order for precipitation enhancement in IR of Iran," *Journal of Weather Modification*, vol. 39, no. 1, pp. 87–95, 2007.

[23] M. J. Manton and L. Warren, "A confirmatory snowfall enhancement project in the Snowy Mountains of Australia. Part II: primary and associated analyses," *Journal of Applied Meteorology and Climatology*, vol. 50, no. 7, pp. 1448–1458, 2011.

[24] D. Breed, R. Rasmussen, C. Weeks, B. Boe, T. Deshler, and C. Weeks, "Evaluating winter orographic cloud seeding: design of the Wyoming weather modification pilot project (WWMPP)," *Journal of Applied Meteorology and Climatology*, vol. 53, no. 2, pp. 282–299, 2014.

[25] B. Pokharel, B. Geerts, X. Jing et al., "The impact of ground-based glaciogenic seeding on clouds and precipitation over mountains: a multi-sensor case study of shallow precipitating orographic cumuli," *Atmospheric Research*, vol. 147-148, pp. 162–182, 2014.

[26] G. A. Isaac, R. S. Schemenauer, C. L. Crozier et al., "Preliminary tests of a cumulus cloud seeding technique," *Journal of Applied Meteorology*, vol. 16, no. 9, pp. 949–958, 1977.

[27] J. J. Schroeder, D. A. Kristovich, and M. R. Hjelmfelt, "Boundary layer and microphysical influences of natural cloud seeding on a lake-effect snowstorm," *Monthly Weather Review*, vol. 134, no. 7, pp. 1842–1858, 2006.

[28] D. Rosenfeld, "New insights to cloud seeding for enhancing precipitation and for hail suppression," *Journal of Weather Modification*, vol. 39, no. 1, pp. 61–69, 2007.

[29] C. Lee, K. Chang, J. Cha et al., "Estimation for the economic benefit of weather modification enhancement and fog dissipation," *Atmosphere*, vol. 20, no. 2, pp. 187–194, 2010.

[30] National Institute of Meteorological Sciences, *Development of Application Technology on Atmospheric Research Aircraft (IV)*, National Institute of Meteorological Sciences, Jeju-do, Korea, 2020.

[31] R. A. Kerr, "Cloud seeding: one success in 35 years," *Science*, vol. 217, no. 4559, pp. 519–521, 1982.

[32] M. Garstang, R. Bruintjes, R. Serafin et al., "Weather modification: finding common ground," *Bulletin of the American Meteorological Society*, vol. 86, no. 5, pp. 647–656, 2005.

[33] National Research Council, *Critical Issues in Weather Modification Research*, National Academies Press, Washington, DC, USA, 2003.

[34] B. Pokharel, B. Geerts, X. Jing, K. Friedrich, K. Ikeda, and R. Rasmussen, "A multi-sensor study of the impact of ground-based glaciogenic seeding on clouds and precipitation over mountains in Wyoming. Part II: seeding impact analysis," *Atmospheric Research*, vol. 183, pp. 42–57, 2017.

[35] L. O. Grant and P. W. Mielke, "A randomized cloud seeding experiment at Climax, Colorado 1960-1965," *Fifth Berkley Symposium on Mathematical Statistic and Probability*, vol. 5, pp. 115–131, 1967.

[36] P. W. Mielke, L. O. Grant, and C. F. Chappell, "An independent replication of the Climax wintertime orographic cloud seeding experiment," *Journal of Applied Meteorology*, vol. 10, no. 6, pp. 1198–1212, 1971.

[37] A. L. Rangno and P. V. Hobbs, "Further analyses of the Climax cloud seeding experiments," *Journal of Applied Meteorology*, vol. 32, no. 12, pp. 1837–1847, 1993.

[38] R. M. Rasmussen, S. A. Tessendorf, L. Xue et al., "Evaluation of the Wyoming Weather Modification Pilot Project (WWMPP) using two approaches: traditional statistics and ensemble modeling," *Journal of Applied Meteorology and Climatology*, vol. 57, no. 11, pp. 2639–2660, 2018.

[39] A. Gagin and J. Neumann, "The second Israeli randomized cloud seeding experiment: evaluation of the results," *Journal of Applied Meteorology*, vol. 20, no. 11, pp. 1301–1311, 1981.

[40] D. Rosenfeld and H. Farbstein, "Possible influence of desert dust on seedability of clouds in Israel," *Journal of Applied Meteorology*, vol. 31, no. 7, pp. 722–731, 1992.

[41] T. Al Hosari, A. Al Mandous, Y. Wehbe et al., "The UAE cloud seeding program: a statistical and physical evaluation," *Atmosphere*, vol. 12, no. 8, p. 1013, 2021.

[42] S. Kwon, S. H. Jung, and G. Lee, "Inter-comparison of radar rainfall rate using Constant Altitude Plan Position Indicator and hybrid surface rainfall maps," *Journal of Hydrology*, vol. 531, pp. 234–247, 2015.

[43] S. Chae, K. Chang, S. Seo et al., "Numerical Simulations of airborne glaciogenic cloud seeding using the WRF model with the modified morrison scheme over the Pyeongchang Region

in the winter of 2016," *Advances in Meteorology*, vol. 2018, Article ID 8453460, 15 pages, 2018.

[44] K. Friedrich, K. Ikeda, S. A. Tessendorf et al., "Quantifying snowfall from orographic cloud seeding," *Proceedings of the National Academy of Sciences*, vol. 117, no. 10, pp. 5190–5195, 2020.

[45] Y. Ro and C. Yoo, "Consideration of rainfall intermittency and log-normality on the merging of radar and the rain gauge rain rate," *Journal of Hydrology*, vol. 589, pp. 125178–125212, 2020.

[46] C. Yoo, C. Park, J. Yoon, and J. Kim, "Interpretation of mean-field bias correction of radar rain rate using the concept of linear regression," *Hydrological Processes*, vol. 28, no. 19, pp. 5081–5092, 2014.

[47] J. Kim and C. Yoo, "Use of a dual Kalman filter for real-time correction of mean field bias of radar rain rate," *Journal of Hydrology*, vol. 519, pp. 2785–2796, 2014.

[48] C. K. Kim, S. S. Yum, and Y. S. Park, "A numerical study of winter orographic seeding experiments in Korea using the weather research and forecasting model," *Meteorology and Atmospheric Physics*, vol. 128, no. 1, pp. 23–38, 2016.